ORIGINAL PAPER

Impact of advection on two-source energy balance (TSEB) canopy transpiration parameterization for vineyards in the California Central Valley

William P. Kustas[1] · Hector Nieto[2,3] · Omar Garcia-Tejera[4] · Nicolas Bambach[5] · Andrew J. McElrone[6,7] · Feng Gao[1] · Joseph G. Alfieri[1] · Lawrence E. Hipps[8] · John H. Prueger[9] · Alfonso Torres-Rua[10] · Martha C. Anderson[1] · Kyle Knipper[11] · Maria Mar Alsina[12] · Lynn G. McKee[1] · Einara Zahn[13] · Elie Bou-Zeid[13] · Nick Dokoozlian[12]

Abstract

Water conservation efforts for California's agricultural industry are critical to its sustainability through severe droughts like the current one and others experienced over the last two decades. This is most critical for perennial crops, such as vineyards and orchards, which are costly to plant and maintain and constitute a significant fraction of the regional water use. It is no longer feasible to access groundwater for irrigation to replace deficit surface water resources during drought due to a significant overdraft of aquifers and new regulation limiting its use. To achieve significant water savings, the actual crop water use or evapotranspiration (ET) needs to be mapped from field to regional scales on a daily basis. This can only be achieved using remote sensing-based models, particularly thermal-based energy balance models that are sensitive to deficit irrigation conditions. The two-source energy balance (TSEB) model has been successfully applied over vineyards in California, but challenges still remain. In particular, much of the irrigated cropland in the California Central Valley is affected by advection of hot dry air masses from surrounding non-irrigated areas and the TSEB model appears to need modifications to adequately estimate ET under such conditions, as well as the partitioning between evaporation and transpiration. This study investigates the application of the TSEB model, using local observations in a vineyard having significant advection. Four versions of the transpiration algorithm in TSEB are applied and evaluated with tower eddy covariance measurements spanning 4 growing seasons. The results suggest the performance of the original transpiration algorithm based on Priestley–Taylor used in TSEB is satisfactory in all but the most extreme advective conditions, while a transpiration algorithm based on Shuttleworth–Wallace with a canopy resistance formula, which relates maximum stomata conductance to vapor pressure deficit (VPD), performs well in all cases. These modifications have potential for improving regional applications of the TSEB model in support of water management in the Central Valley.

Introduction

California's Central Valley is one of the richest agricultural regions in the world. In the U.S., over a third of the country's vegetables and two-thirds of the country's fruits and nuts are grown in California (https://www.cdfa.ca.gov/Statistics/). However, this rich agricultural region, which is largely irrigated, is facing serious water shortages due to drought and overdraft of its aquifers. During the recent intense drought of 2012–2016, surface water shortages in

agriculture were offset by intensive groundwater pumping. The resulting overdraft caused significant land subsidence and loss of groundwater resources. In response, California enacted and passed into law in 2015 the Sustainable Groundwater Management Act (SGMA; https://water.ca.gov/programs/groundwater-management/sgma-groundwater-management), which requires local Groundwater Sustainability Agencies (GSAs) to be formed and Groundwater Sustainability Plans (GSPs) to be prepared with the goal of achieving sustainable groundwater management. This necessitates developing techniques for water conservation and groundwater recharge. SGMA will cover 127 medium and high-priority groundwater sub-basins in California, including over 100 sub-basins where chronic overdraft is occurring. The current drought in 2021 is leading

✉ William P. Kustas
Bill.Kustas@ars.usda.gov

Extended author information available on the last page of the article

to severe water shortages throughout the western U.S. and reducing or restricting water use for agriculture. The agriculture industry is looking for technological innovations that will help dramatically improve water use efficiency, conserve water, and lead to sustainable production, while remaining economically viable.

Development of water conservation measures is most critical for perennial crops, such as vineyards and orchards, which require significant upfront investment. Wine producers have realized that implementing significant improvements in irrigation efficiency and water conservation while maintaining yield and quality will require development of technologies to monitor water use at field, landscape, and regional scales. This realization led E&J Gallo, Inc. to partner with USDA's Agricultural Research Service to develop satellite-based remote sensing tools to track crop water use and stress. The GRAPEX (Grape Remote sensing Atmospheric Profile Evapotranspiration eXperiment) project, with support from USDA and NASA, has the goal of providing wine grape producers, and in the longer term, fruit and nut orchard growers, with the tools to generate robust high-resolution maps of actual evapotranspiration (ET), or crop water use, that can be used to guide irrigation management decisions (Kustas et al. 2018). These tools will have the advantage over current approaches for assessing water needs by being applicable year-round and by providing water use information with higher spatial and temporal detail.

Research results from GRAPEX were first published in a special issue in *Irrigation Science* (Kustas et al. 2019a), indicating robust results using airborne-based unmanned aerial systems (UASs) and satellite-based ET modeling techniques modified using GRAPEX-supported ground validation data. These ET products, derived from land surface temperature (LST), are showing utility for monitoring ET and vine stress (Knipper et al. 2019); however, there are issues that require further research and model refinements.

The two-source energy balance (TSEB) model, originally proposed by Norman et al. (1995) (see available Python code online at https://github.com/hectornieto/pyT-SEB), is central to the vineyard ET estimates derived in the GRAPEX project. The TSEB model is susceptible to enhanced ET estimates caused by advective conditions, which are common in irrigated agricultural regions in the western U.S. and abroad. As a result, the original Priestley–Taylor formulation of plant potential transpiration (i.e., commonly used value of 1.26 for the alpha parameter; Kustas and Norman 1999) may require an increase based on the evaporative demand using a metric such as vapor pressure deficit (VPD) (Agam et al. 2010). For irrigated areas in arid landscapes, other transpiration formulations for TSEB have been proposed using Penman–Monteith (Colaizzi et al. 2012, 2014), as well as refinements to below canopy radiation extinction and wind profile algorithms specific to the characteristic wide row and orientation and the non-uniform vegetation biomass distribution in vineyards (Nieto et al. 2019a; b).

In this paper we explore the effect on estimating ET under different levels of advection using the traditional Priestley–Taylor approach (Priestley and Taylor 1972) for transpiration but with a modification for the original alpha parameter, α_{PT} of 1.26. This was applied to improve PT-JPL (Priestley–Taylor Jet Propulsion Laboratory) ET model (Fischer et al. 2008) estimates for arid and semiarid environments where advection is prevalent, as part of the OpenET project (Melton et al. 2022). The α_{PT} parameter was modified using an evaporative demand metric based on based on the ratio of the American Society of Civil Engineering (ASCE) reference ET (ET_O) and the original Priestley-Taylor formulation for a wet surface ET_W, following principles derived from the complementary relationship of evaporation (Brutsaert and Stricker 1979; Brutsaert 1982; Kahler and Brutsaert 2006; Szilagyi 2007; Huntington et al. 2011). The ASCE reference ET_O and Priestley–Taylor ET_W estimates were developed using the gridMET dataset described in Melton et al. (2022). The α_{PT} adjustment map was computed as the ratio of the growing average bias corrected ET_O to the growing season average ET_W. Please refer to Melton et al. (2022) for details (see also https://openetdata.org/methodologies/). This version of TSEB (i.e., TSEB-PT$_{clim}$) represents the adjustment to the alpha parameter based on the climatological values derived from this approach.

Colaizzi et al. (2012, 2014) developed another modification to handle transpiration in the TSEB model that appears to better accommodate advective conditions than the Priestley–Taylor method of Kustas and Norman (1999). This approach uses the Penman–Monteith formulation for plant transpiration based on an assumed constant minimum stomatal resistance (TSEB-PM$_{Rc,min}$). We also examine an alternative minimum stomatal resistance formulation, dependent on a VPD formulation and based on the studies by Monteith (1995) and Leuning (1995), within a modified TSEB framework that explicitly accounts for the partial canopy condition through the use of the Shuttleworth-Wallace model (TSEB-SW$_{Rc,VPD}$). These different TSEB formulations are applied to local tower-based hemispherical LST observations from a longwave radiometer over a vineyard in a strongly advective environment and compared to eddy covariance tower measurements of ET to identify the optimal formulation.

Approach

The various TSEB formulations described above and applied to vineyards only differ in the transpiration formulation used to initially determine maximum vine transpiration. Here,

we summarize the transpiration formulations for TSEB-PT, TSEB-PT$_{\text{clim}}$, TSEB-PM$_{\text{Rc,min}}$ and TSEB-SW$_{\text{Rc,VPD}}$.

TSEB-PT and TSEB-PT$_{\text{clim}}$

For TSEB-PT and TSEB-PT$_{\text{clim}}$, the transpiration, or latent heat flux from the vine canopy (LE$_C$), is given as follows:

$$LE_C = \alpha_{PT} f_g \frac{\Delta}{\Delta + \gamma} R_{n,C}. \tag{1}$$

Here, α_{PT} is the Priestley–Taylor coefficient (set at the classic value of 1.26 for TSEB-PT), f_g is the fraction of vegetation that is green and hence transpiring, applied to the canopy divergence of net radiation ($R_{n,C}$), Δ is the slope of the saturation vapor pressure versus temperature curve, and γ is the psychrometric constant. For TSEB-PT$_{\text{clim}}$ the ET$_O$/ET$_W$ monthly ratio is nearly constant for the growing season and equals ~ 1.23 in the study area, which yields an $\alpha_{PT} =$ ET$_O$/ET$_W \times 1.26 \sim 1.55$ for use in Eq. (1). The TSEB-PT formulation requires both a solution to the radiative temperature balance and the energy balance with physically plausible model solutions for soil and vegetation temperatures and fluxes. Non-physical solutions typically occur when the canopy is stressed requiring an iterative reduction in α_{PT} until a physical solution is obtained (Kustas and Anderson, 2009). However, TSEB-PT cannot iteratively adjust the initial α_{PT} under enhanced transpiration conditions from advection.

TSEB-PM$_{\text{Rc,min}}$

For details concerning the TSEB-PM$_{\text{Rc,min}}$ transpiration algorithm, the reader is referred to Colaizzi et al. (2012, 2014). Using a Penman–Monteith form, LE$_C$ can also be calculated as:

$$LE_C = f_g \left(\frac{\Delta R_{N,C}}{\Delta + \gamma^*} + \frac{\rho C_P (e_S - e_A)}{r_A (\Delta + \gamma^*)} \right), \tag{2}$$

where ρ is the air density (kg m^{-3}), C_P is the specific heat of air (assumed constant at 1013 J kg^{-1} K^{-1}), $\gamma^* = \gamma(1 + r_C/r_A)$, r_C is the bulk canopy resistance (s m^{-1}), r_A is the aerodynamic resistance between the canopy and the air above the canopy (s m^{-1}), e_S and e_A are the saturation and actual vapor pressures of the air (kPa), respectively, and all other terms are as defined previously. An increase in vapor pressure deficit (VPD $= e_S - e_A$) may be offset by an increase in r_C (and, thus, γ^*) due to stomatal response to environmental factors (Jarvis, 1976; Lohammar et al. 1980; Monteith, 1995); however, Allen et al. (2006) concluded that r_C is generally constant and recommended values of 50 s m^{-1} during the day

and 200 s m^{-1} at night for a reference short crop (i.e., well-watered and full canopy). Therefore, TSEB-PM$_{\text{Rc,min}}$ also uses this constant value at 50 s m^{-1} to be consistent with the original TSEB-PM implementation by Colaizzi et al. (2012, 2014). Increasing VPD while holding r_C constant results in increasing LE$_C$ in Eq. 2, similar to increasing α_{PT} in Eq. 1.

TSEB-SW$_{\text{Rc,VPD}}$

While constant r_C is a reasonable assumption for short reference crops since the limiting factor in such crops is the aerodynamic resistance (r_A), sensitivity of r_C to VPD can play a more significant role in canopy transpiration in taller and/or heterogeneous canopies, and hence aerodynamically rougher and better coupled with the atmosphere, as canopy and aerodynamic resistances are more similar in magnitude (Jarvis and McNaughton 1986). In those cases, it is key to parameterize the stomatal closure with increasing VPD, whose behavior might indeed differ between species and even between varieties (Grossiord et al. 2020).

Accounting for the negative feedback observed between transpiration (T) rates and stomatal closure based on a wide variety of plant level measurements, Monteith (1995) proposed a method to parameterize the relationship between leaf stomatal conductance (g_s) and VPD, based on measurements of transpiration as follows in Eq. (3):

$$g_s = \frac{g_m}{1 + g_m \text{VPD}/T_m}, \tag{3}$$

where g_m is the maximum stomata conductance and T_m is the maximum rate of leaf transpiration. A similar hyperbolic relation between g_s and VPD is shown in Lohammar et al. (1980) and Leuning (1995). Leaf level g_s is then upscaled to canopy resistance (r_C) using LAI and Eq. (4):

$$r_C = \frac{1}{f_t f_g \text{LAI} g_s}, \tag{4}$$

where f_t ranges between 1 and 2 indicating the stomata distribution in the leaves (i.e., 1 for hypostomatous and 2 for amphistomatous leaves).

Values of g_m and T_m are empirically derived in Monteith (1995) by plotting observations of T and VPD, and building a linear regression in the form given in Eq. (5):

$$1/T = \frac{1}{a\text{VPD}} + b, \tag{5}$$

from which $g_m = a$ and $T_m = 1/b$. These two coefficients are considered crop specific, as the sensitivity of stomatal conductance to VPD might differ between species (Grossiord et al. 2020).

This variable r_C as a function of VPD and LAI can be used as input for canopy conductance-based TSEB as in TSEB-PM

instead of using the static $r_C = 50\,\text{s m}^{-1}$. However, in this study, we also incorporated the effect of having partial vegetation cover due to significant interrow spacing between the vine rows. This has the effect that potential transpiration and thus, canopy temperature is linked with the soil sensible and latent heat fluxes, as the soil can be a source of hot and dry (cool and humid) air to the canopy–air interface if soil surface is dry (wet). As such we adopted the Shuttleworth–Wallace approach (Shuttleworth and Wallace 1985) incorporating a soil/substrate evaporation formulation in combination with the canopy transpiration to accommodate an incomplete canopy cover that exists in vineyards and flux and momentum interaction between these two layers. Furthermore, the dual-source Shuttleworth–Wallace model for computing the potential transpiration and minimum canopy temperature allows this approach to be a "seamless" framework, as both TSEB and Shuttleworth–Wallace models share the same resistance scheme in series. This new proposed approach using Shuttleworth and Wallace (1985) energy-combination model in TSEB, TSEB-SW$_{\text{Rc,VPD}}$, estimates the initial canopy transpiration with the following formulation:

$$\text{LE}_C = \frac{\Delta R_{\text{N,C}} + \rho C_P \text{VPD}_0}{\Delta + \gamma \left(1 + \frac{r_C}{r_x}\right)}, \tag{6}$$

where VPD_0 is the atmospheric vapor pressure deficit within the canopy airspace; r_x is the canopy boundary layer aerodynamic resistance to momentum, heat and vapor transport; and r_C is the canopy stomatal conductance computed by Eqs. (3) and (4).

The vapor pressure deficit at canopy source height is computed using Eq. (7) (Shuttleworth and Wallace 1985):

$$\text{VPD}_0 = \text{VPD} + r_a \frac{\Delta (R_N - G) - (\Delta + \gamma)\text{LE}}{\rho C_p}, \tag{7}$$

where r_a is the aerodynamic resistance to turbulent transport, R_N is the surface net radiation, G is the soil heat flux, and LE is the surface bulk latent heat flux, estimated as:

$$\text{LE} = C_C \text{PM}_C + C_S \text{PM}_S. \tag{8}$$

Here, C_C and C_S are weighting factors based on soil and canopy resistances (Eqs. 14 and 15 in Shuttleworth and Wallace 1985), and PM_C and PM_S are the LE estimates of a closed canopy and bare soil, respectively, using the Penman–Monteith equation:

$$\text{PM}_C = \frac{\Delta (R_N - G) + \frac{\rho C_P \text{VPD} - \Delta r_x (R_{\text{N,S}} - G)}{r_a + r_x}}{\Delta + \gamma \left(1 + \frac{r_C}{r_a + r_x}\right)}, \tag{9a}$$

$$\text{PM}_S = \frac{\Delta (R_N - G) + \frac{\rho C_P \text{VPD} - \Delta r_s R_{\text{N,C}}}{r_a + r_s}}{\Delta + \gamma \left(1 + \frac{r_{\text{ss}}}{r_a + r_s}\right)}, \tag{9b}$$

where r_s is the soil boundary layer (aerodynamic) resistance to turbulent transport and r_{ss} is the near-surface soil resistance to vapor transport, which is normally a function of near-surface soil moisture.

In a first step of TSEB-SW$_{\text{Rc,VPD}}$, we assume that a canopy transpires at potential rate and soil surface is still wet, therefore g_s (r_C) is set to maximum stomatal conductance (minimum canopy resistance) and r_{ss} is set to minimum near-surface soil resistance. From this first guess of LE$_C$, canopy temperature (T_C) is retrieved and soil temperature (T_S) is computed by inverting Eq. (10).

$$T_{\text{rad}}^4 = f_C(\theta)T_C^4 + \left(1 - f_C(\theta)\right)T_S^4, \tag{10}$$

where T_{rad} is the radiometric *LST* observed at view zenith angle θ and $f_C(\theta)$ is the fraction of vegetation observed at the sensor's view zenith angle (in our study it is assumed $\theta = 0$; see Eq. 13). The value of $f_C(\theta)$ is typically estimated as an exponential function of LAI, which includes a clumping factor or index Ω for canopies where the LAI is concentrated for sparsely distributed plants or for organized canopies such as row crops (Kustas and Norman 1999), and has the following form for a canopy with spherical leaf distribution:

$$f_C(\theta) = 1 - \exp\left(\frac{-0.5\Omega\text{LAI}}{\cos\theta}\right). \tag{11}$$

However due, to the unique vertical canopy structure and wide row width relative to canopy height of vineyards, a new method to derive Ω had to be developed that was both based on a simplified geometric model developed by Parry et al. (2019) that also yielded robust radiation extinction estimates for vine canopies. Similarly, as in TSEB-PM (and TSEB-PT), if LE$_S$ is negative at this stage the TSEB-SW$_{\text{Rc,VPD}}$ model iteratively decreases g_s, as well as increases r_{ss} (i.e., a dryer soil surface), until both LE$_S$ and LE$_C$ become non-negative for daytime conditions.

Estimating hourly and daily ET These four versions of the TSEB were tested at hourly timesteps using in situ meteorological and LST measurements from a flux tower. We also test a remote sensing method for upscaling instantaneous TSEB LE derived from Landsat LST to a daily total LE (LE$_{\text{day}}$), as recently applied over the California vineyards (Knipper et al. 2020), using the 10:30 local time TSEB estimate coinciding nominally with Landsat overpass time. The method takes the ratio of instantaneous to daily insolation ($R_{\text{S}\downarrow}$) at the overpass time (t) with the following formulation:

Table 1 Information on vineyard properties and biophysical information for RIP760 block containing the GRAPEX flux tower

Geographic information	
Vineyard	(RIP760) Madera County
Height above sea level (m)	58
Topography	Flat
Soil type	Sandy loam
Vine information	
Vine variety	Chardonnay
Year planted	2010
Bud break	3/10–3/23
Flowering/fruit set	4/21–4/30
Veraison	7/14–7/23
Harvest	8/8–8/29
Vineyard architecture	
Row orientation	East–West
Trellising method	Double vertical
Row width	2.74 m
Planting interval	1.83 m
First and (second) cordon height	1.20 (1.70) m
Vine canopy height (April–September)	1.5–2.5 m
Vine canopy width (April–September)	0.5–1.8 m
Cover crop information	
Cover crop type	Annual grasses
Cover crop width	1.2 m
Agronomic and management information	
Cover crop management	Mowed once or twice in April/May
Irrigation system	In line dripper (3 emitters per vine at 0.52 gallons per hour each)
GRAPEX specific information	
Date of initial tower deployment	May 9, 2017

$$LE_{day} = LE_{t2} \frac{R_{S\downarrow,day}}{R_{S\downarrow,t}}. \tag{12}$$

This insolation technique has proven generally reliable, with lower bias and sensitivity to errors in retrieval estimates when compared to other techniques (Cammalleri et al. 2014; Nassar et al. 2021), but may underestimate daily ET for irrigated crops under strongly advective conditions (Colaizzi et al. 2006). Finally extrapolated daily latent heat fluxes (in W m^{-2}) are converted to daily evaporation rates (mm day^{-1}) considering the mean daily air temperature for the calculation of both the latent heat of vaporization (λ) and water density (ρ_w) [ET = LE/($\rho_w \lambda$)].

Materials and methods

Experiment site and tower measurements

The vineyard site (RIP760) is located in the California Central Valley 30 km west of Fresno, CA, in Madera County and is encompassed by multiple vineyard blocks and orchards in the surrounding landscape. This region of the Central Valley is at the drier and hotter extent of where wine grapes are grown. The RIP760 vineyard block is 31 ha in size containing *Vitis vinifera* Chardonnay variety grapevines trained on double vertical trellis, and drip irrigated. Information pertaining to vineyard geography, vine phenology, vineyard architecture and agronomic properties of the vineyard block is listed in Table 1. In brief, vines were planted in 2009 with 1.83 m vine spacing and 2.74 m row spacing and have an East–West row orientation. RIP760 is on relatively flat terrain and has a cover crop planted yearly in the fall after harvest, which is mowed and senescent during most of the vine growing (dry) season. Figure 1 illustrates the field site location along with photos showing the tower and vine and interrow conditions during the growing season.

Measurements at all sites include turbulence and mean profile measurements of wind, surface energy balance flux estimates, temperature and water vapor, as well as periodic ground-based biophysical measurements such
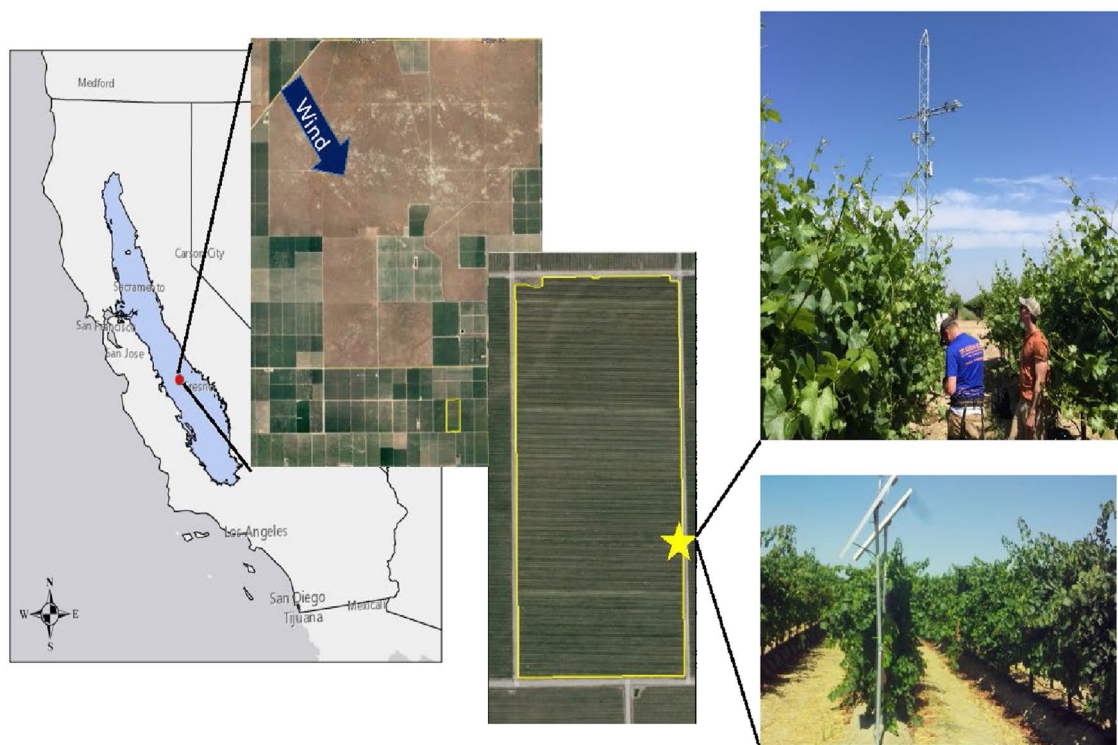
Fig. 1 Location of the vineyard study site (RIP760) within the California Central Valley region. In the blowups from Google Maps, there is a large fallow area upwind with the tower location (yellow star) to maximize the fetch from RIP720 within the yellow boundary. The photos of the vineyard and tower were taken in early May (top) and later in the growing season in July (bottom) (colour figure online)

as LAI, leaf water potential, and gas exchange. LAI was measured in situ using optical non-destructive methods (see White et al. 2018). The sampling methodology for leaf water potential and gas exchange is described in Nieto et al. (2022) but are not used in this study.

A flux tower at RIP760 was installed in May of 2017 using eddy covariance (EC) systems from Campbell Scientific,[1] Inc. Logan Utah. The EC150 or IRGASON system measuring water vapor/carbon dioxide together with a CSAT3 three-dimensional sonic anemometer compute latent and sensible heat fluxes, net carbon exchange and momentum flux at approximately 5.5 m above ground level (a.g.l.) facing due west. The EC system collect data at 20 Hz producing 15 min average fluxes as well as temperature, vapor pressure and wind speed. Post processing of the 20-Hz data for fully correcting the high frequency data is described by Alfieri et al. (2019). Additional instrumentation includes a four-component radiometer (NR01 Net Radiometer Hukseflux, Delft, Netherlands) mounted 6.3 m a.g.l. Also included is a combined

humidity and temperature sensor HC2S3 with radiation shield from Campbell Scientific and an aspirated TS-100 shield (Apogee, Logan Utah) with EE08 temperature and humidity sensor (E + E Eletronik, Langwiesen, Austria) mounted at 5.5 m a.g.l., and a tipping bucket rain gauge (TE525, Texas Electronics, Dallas, Texas) is installed at 1 m above the vine canopy. In the interrow several meters from the tower there are five soil heat flux plates (HFT-3, Radiation Energy Balance Systems, Bellevue, Washington) evenly distributed across the interrow at a depth of 8 cm. Each heat flux plate includes two thermocouples buried at depths of 2 and 6 cm and a soil moisture sensor (HydraProbe, Stevens Water Monitoring System, Portland, Oregon) buried at 5 cm depth to account for storage term above the soil heat flux plates. A description of these soil measurements is in Agam et al. (2019).

The tower observations of daytime average H for the different years for May through August show that the lowest H values occurred in 2020 followed by 2017 with 2018 and 2019 being similar (Fig. 2). For daytime average LE (Fig. 2), this generally results in slightly higher LE values observed in 2020, followed by 2017, although the differences are not as apparent as with H. The atmospheric demand (reference ET, incoming solar radiation, air temperature, wind and vapor pressure deficit) depicted in
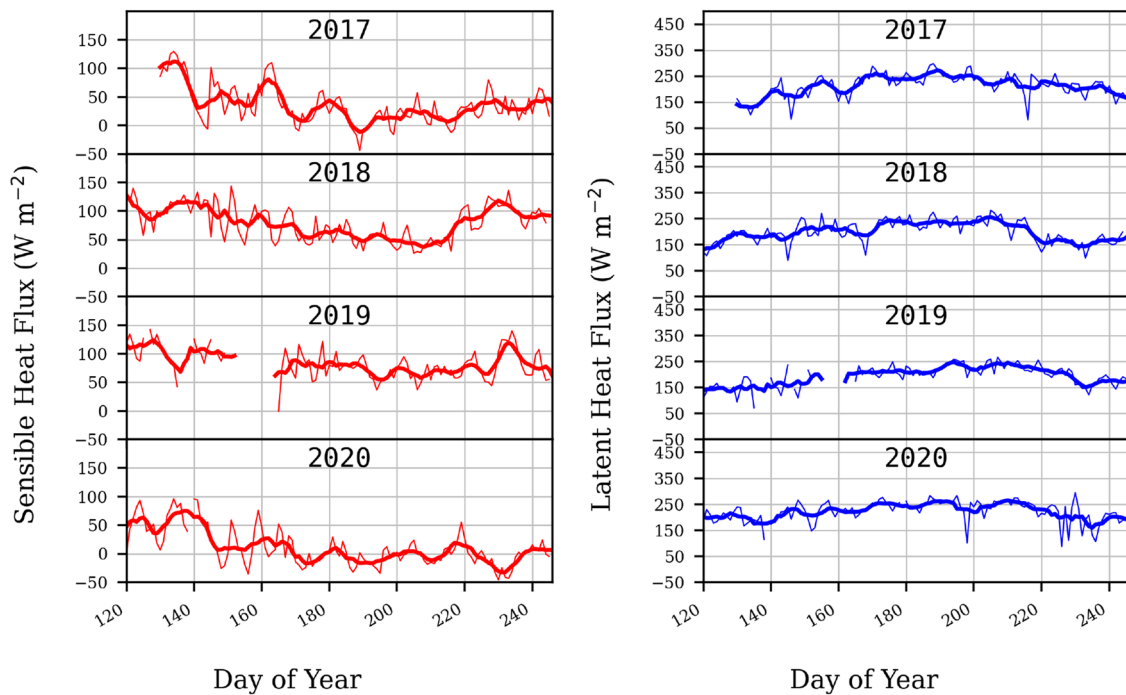
Fig. 2 Measured daytime average sensible heat flux (*H*) and latent heat flux (LE) from eddy covariance towers from May through end of August indicating lowest values in *H* with cases where *H* < 0 occurred during 2017 and 2020 growing seasons which corresponded to higher LE values. Thin lines represent daily flues, while the thicker curves are the 7-day moving average (colour figure online)

Fig. 3 from the nearest CIMIS weather station (Station 80 at Fresno State; https://cimis.water.ca.gov/Stations.aspx) for the different years does not show a trend in any of the quantities, suggesting changes in evaporative demand was not a major factor in the flux variability between years. Instead, it appears that the management decisions may have been a key factor in causing the relatively large changes in *H* observed especially in 2020 and to some extent in 2017. Although the irrigation data were not well documented or monitored until 2019, records indicate that 2020 had significant irrigation early in the growing season in April and May, setting up for significant vine growth or leaf area/biomass.

Analysis of satellite and ground-based measurements of vegetation indices also indicate higher biomass in both 2017 and 2020 than in 2018 and 2019. Figure 4 shows cumulative plots of the enhanced vegetation index (EVI) for a 3 × 3 30 m pixel grid (i.e., 90 × 90 m total area) in the typical upwind fetch of the flux tower from satellite data (Fig. 4), showing highest growth rates in 2020 followed by 2017. To generate these plots, daily EVI time series were generated from Harmonized Landsat and Sentinel-2 (HLS) data (Claverie et al. 2018), smoothed and interpolated using the Savitzky–Golay filter with a flexible moving window strategy as described in Gao et al. (2020), and then accumulated over the months of July to August for the 4 years (2017–2020). EVI has greater sensitivity for high biomass vegetation than the normalized

difference vegetation index (NDVI) and is less affected by saturation problems (Huete et al. 2002). Years with greater biomass, and thus greater ET when there was sufficient plant available water, sets the stage for significantly higher ET via greater transpiration under similar advective conditions or evaporative demand as other years having less vine leaf area.

Model inputs

The four different transpiration parameterizations for TSEB were run using hourly inputs for wind, air temperature, vapor pressure, and solar radiation obtained from the RIP760 tower. Key remote sensing inputs to the TSEB include LST, used in Eq. 10, and LAI, used in the partitioning between the soil and canopy. The approach of Gao et al. (2020) based on machine learning, which was recently modified for vineyards by Kang et al. (2022), was applied to generate daily LAI maps at 30 m resolution over the RIP760 using Landsat and Sentinel-2 surface reflectance, ground-based observations and the MODIS LAI products. LST was estimated using the tower-based upwelling longwave radiometer 4-way net radiometer. This is a hemispherical LST (T_{RH}), which represented T_{rad} observed at nadir and was computed based on the following expression:
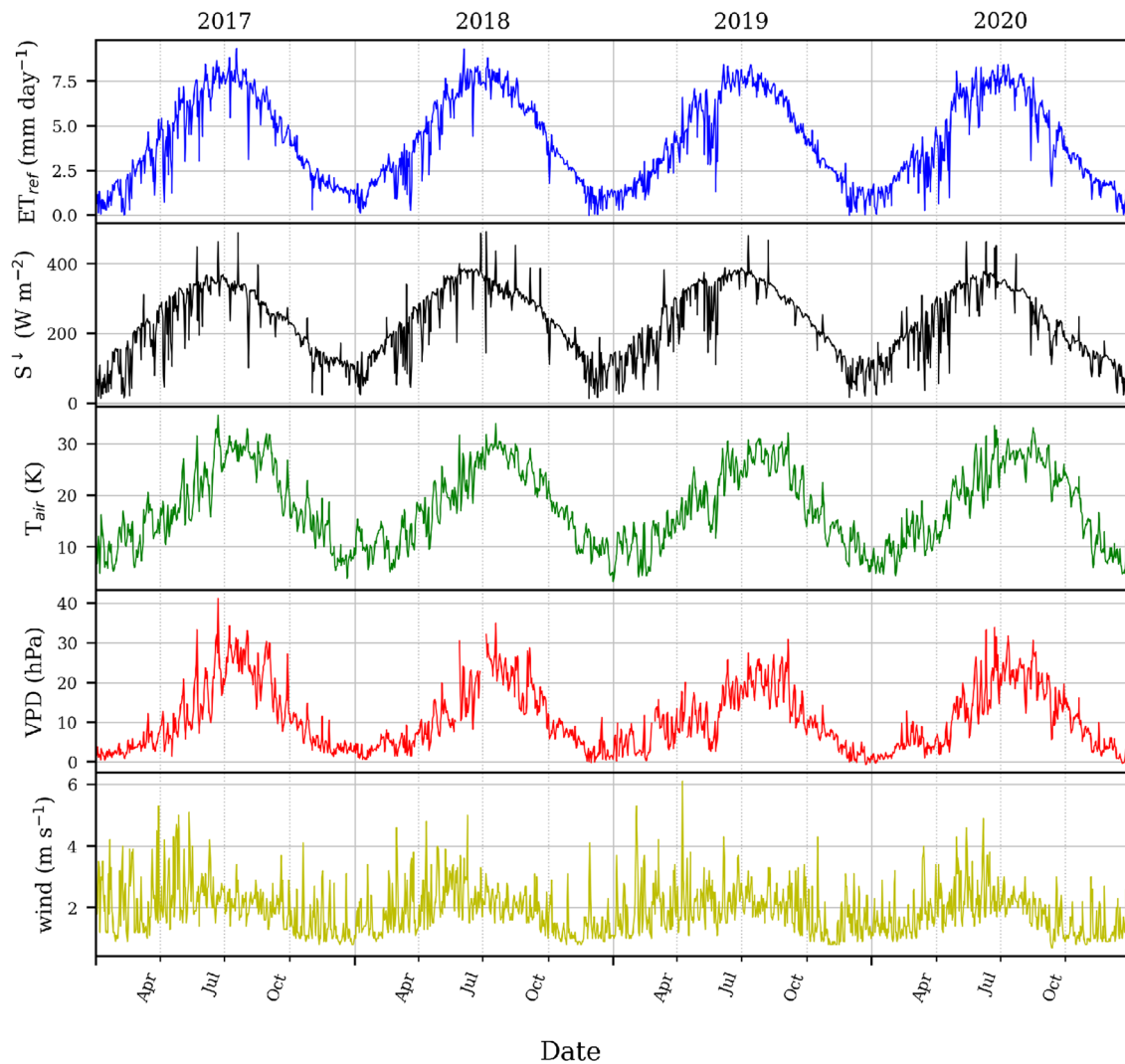
Fig. 3 Daily-averaged reference ET (ET$_{ref}$), incoming solar ($S^{\downarrow}$), air temperature (T_{air}), vapor pressure deficit (VPD), and wind speed (wind) observations from the CIMIS station at Fresno State for the years 2017–2020 (colour figure online)

$$T_{RH} = \left(\frac{\left[R_{L\uparrow} - \left(1 - \varepsilon_H \right) R_{L\downarrow} + R_{Latm} \right]}{\sigma \varepsilon_H} \right)^{1/4}, \tag{13}$$

where $R_{L\uparrow}$ is the upwelling longwave radiation measurement, $R_{L\downarrow}$ is the downwelling longwave radiation, R_{Latm} is the atmospheric longwave contribution from ground to sensor height, σ is Stefan–Boltzmann constant and ε_H is the hemispherical emissivity estimated from weighting the fractional vegetation cover estimates (f_C) based on a relationship with LAI estimated clumping factor (Kustas et al. 2019b) and

assumed emissivity of the canopy (0.99) and soil/cover crop (0.94), i.e., $\varepsilon_H = 0.99(f_C) + 0.94(1 - f_C)$. Given the relatively small path length of the longwave sensor from the ground, it was assumed $R_{Latm} \sim 0$.

Vine plant parameters for the TSEB model were estimated from biophysical data collected over the years from Intensive Observation Periods (Kustas et al. 2018) at different phenological stages (see Table 1).
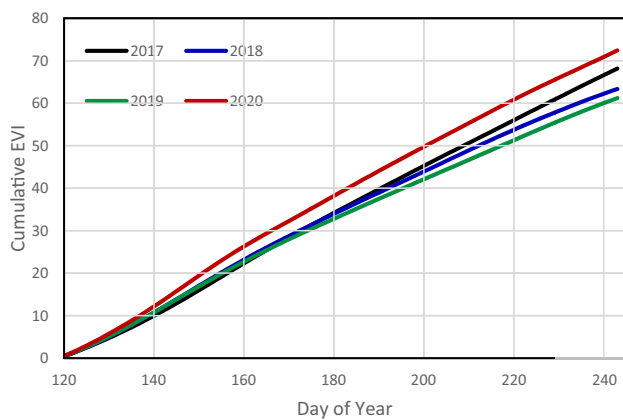
Fig. 4 Cumulative enhanced vegetation index (EVI) within the tower footprint (3×3 30 m pixels) in the northwest quadrant providing an indication of cumulative green biomass from May through end of August for the 2017 through 2020 growing seasons (colour figure online)
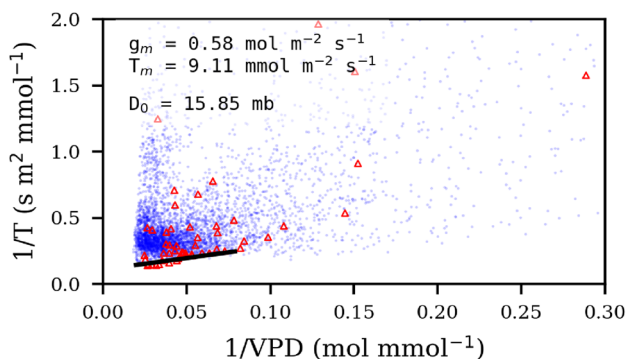
Fig. 5 Reciprocal of effective leaf transpiration rate, T (s m^{-2} $mmol^{-1}$) vs. the reciprocal vapor pressure deficit, VPD, expressed in molar fraction (mol $mmol^{-1}$). The straight line represents the linear regression of the point cloud lower envelope, from which g_m, T_m and $D_0 = g_m/T_m$ are obtained. The lower envelope is estimated by the 1% percentile of the $1/T$ values after grouping the VPD/T pairs in 30 bins. The blue dots are from measurements in RIP720 while the red triangles are measurements from RIP760. The point cloud above the fitted line represents the cases in which stomata conductance is also limited by other factors such as temperature, irradiance and/or soil moisture deficit (colour figure online)

Parameterization of transpiration equation in TSEB-SW$_{Rc,VPD}$

To build the linear regression of Eq. (5), it is first required to work at leaf scale. Therefore, the estimated canopy transpiration from the eddy covariance tower is (T_{EC}) first downscaled to an effective leaf transpiration rate using the satellite LAI ($T_{leaf} = T_{EC}/LAI$). The value of T_{EC} was estimated for a nearby vineyard of a different variety using a combination of relaxed-eddy accumulation and quadrant analysis (Thomas et al. 2008); and a novel approach that

relies only on quadrant analysis using the high frequency eddy covariance data (Zahn et al. 2022). Although the estimation of T_{EC} was performed for a different vine variety (Merlot), it was assumed the derived relationship reflected the general response of vine leaf conductance to VPD and that the sensitivity of the TSEB-SW$_{Rc,VPD}$ formulation of canopy transpiration would not be highly sensitive to the coefficients derived from Eq. (5). In fact, these measurements showed that, under advective conditions (i.e., $H < 0$ and Rn > 100 W m^{-2}), transpiration exceeded by ~ 30% the available surface energy (Rn-G) in both vineyards.

The linear relationship between the reciprocals of VPD and maximum T only appears when VPD is the main limiting factor to stomata closure (Monteith 1995), and hence this linear relationship is derived from the lower envelope of the $1/T$ vs. $1/VPD$ scatterplot for all daytime EC observations under relatively high VPD values.

The scatterplot between the reciprocals of the estimated leaf effective transpiration and VPD is shown in Fig. 5 using the T_{EC} data derived from Zhan et al. (2022) from the adjacent vineyard RIP720. The straight line in Fig. 5 is computed from the linear regression of the lower envelope of the $1/T$ vs $1/VPD$ point cloud, and its regression parameters are used to calculate g_m (0.58 mol m^{-2} s^{-1}) and T_m (9.11 mmol m^{-2} s^{-1}). The D_0 parameter for the equivalent Leuning (1995) formulation is also derived from the site mean atmospheric pressure, and variables g_m and T_m ($D_0 = \bar{p}g_m/T_m = 15.85$ mb). Application of the partitioning techniques for several days of 20 Hz eddy covariance data from RIP760 spanning a range of advective to non-advective cases indicates the regression equation is also representative of the $1/T$ vs $1/VPD$ relationship for RIP760 as points fall along the line derived from RIP720 data (Fig. 5). In fact, TSEB-SW$_{Rc,VPD}$ was also applied with different coefficients than those shown in Fig. 5 derived directly from the $1/T$ vs $1/VPD$ relationship for RIP760, with $g_m = 0.69$ mol m^{-2} s^{-1}, $T_m = 8.92$ mmol m^{-2} s^{-1} and $D_0 = 13.01$ mb. There was virtually no change in the results that are shown below, but in order to ensure using an independent dataset for this calibration and prove the applicability of this approach among varieties, we used the values in Fig. 5 calibrated for RIP720 in this study.

Closure corrections

There may be many factors that result in a lack of energy balance closure between the available energy (Rn-G) and the turbulent fluxes H and LE, and debate continues on what are the key factors that affect closure and if and how various closure methods should be applied (Mauder et al. 2020). Therefore, we have taken the approach of showing modeled-measured differences using commonly applied closure techniques suggested by Twine et al. (2000) assuming the
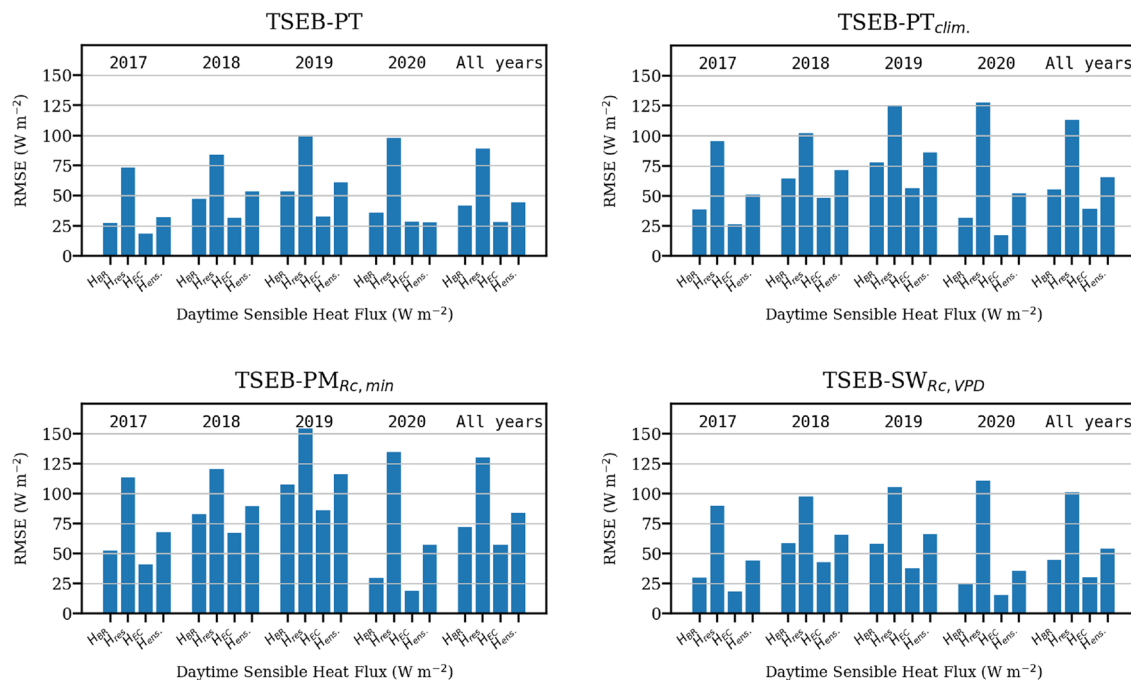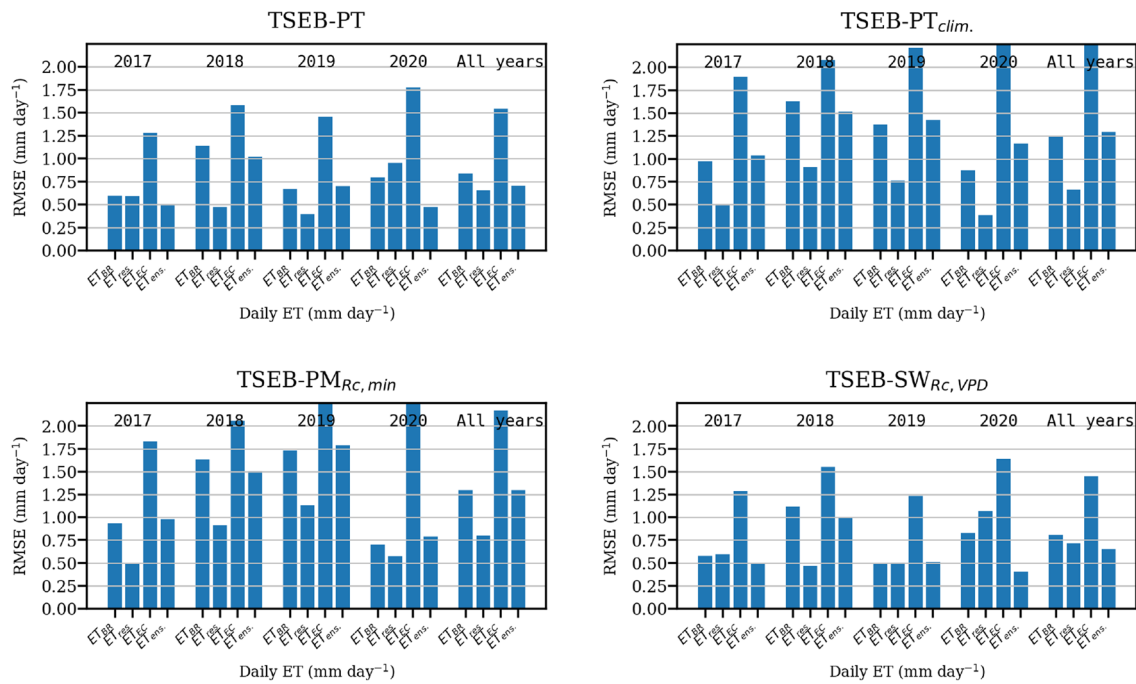
Fig. 6 The RMSE statistics in average daytime sensible heat flux, H, for the four versions of the transpiration formulation in TSEB. The RMSE values are computed using tower H observations with closure by the Bowen ratio (H_{BR}), and residual (H_{RES}) methods, unclosed (H_{EC}) and an ensemble (average) of the three H estimates (H_{ENS} (colour figure online)

underestimation is solely in the latent heat flux (residual) or the undermeasurement is from both H and LE and so the Bowen ratio H/LE is assumed to be correct and preserved in partitioning the missing energy. Alternatively, some have suggested it is largely an undermeasurement of H (Liu et al. 2011; Xu et al. 2017). Hence the statical differences reported will include unclosed H and LE (H_{EC} and LE_{EC}, respectively) closed by residual for both LE and H (LE_{res} and H_{res}, respectively) and by Bowen ratio (LE_{BR} and H_{BR}, respectively) methods. While other methods have also been recommended (Mauder et al. 2020), an uncertainty analysis of closure methods by Bambach et al. (2022) for the GRAPEX vineyards suggests the model-measured comparisons performed here encompass the possible variation in measured fluxes. So, model performance will be evaluated by comparing the difference statistics with the ensemble (average of all three methods), which is assumed to represent the best estimate of observed H and LE (H_{ens}, LE_{ens}).

Results

The four modeling approaches were applied with the RIP760 tower data input of wind speed, incoming radiation, vapor pressure, the derived hemispherical LST, T_{RH}, and LAI from the remote sensing retrievals described above. The root mean square error (RMSE) statistics for each modeling approach are shown in Fig. 6 as bar graphs for the daytime average sensible heat flux H ($R_{S\downarrow} > 0$ W m^{-2}) using the two closure methods described above along with the unclosed H measured by the eddy covariance system as well as the average or ensemble of the three, which is assumed to be closest to the actual/true H. Since the TSEB model computes H directly, the RMSE statistic for this flux is considered the most direct evaluation of model performance. The results illustrated in the figure suggest the lowest RMSE values are generally with either TSEB-PT or TSEB-SW$_{Rc,VPD}$. The only exception is in 2020 where TSEB-PT$_{clim}$ and TSEB-PM$_{Rc,min}$ yielded similar RMSE using unclosed H_{EC}.

Fig. 7 The RMSE statistics in daily ET for the four versions of the transpiration formulation in TSEB. The RMSE values are computed using tower ET observations with closure by the Bowen ratio (ET_{BR}), and residual (ET_{RES}) methods, unclosed (ET_{EC}) and an ensemble (average) of the three ET estimates (ET_{ENS}) (colour figure online)

When evaluating the daily ET values with the different TSEB versions using the extrapolation formula, Eq. (11), the lowest RMSE values (Fig. 7) are generally with either TSEB-PT or TSEB-SW$_{Rc,VPD}$ using all three tower ET estimates including the ensemble, with only exception being in 2020 where TSEB-PT$_{clim}$ and TSEB-PM$_{Rc,min}$ yielded slightly lower RMSE values using ET$_{res}$ as the validation data.

In Tables 2 and 3 the various statistical measures of model performance are listed for estimating daytime average H and daily ET, respectively, using the different transpiration algorithms in TSEB versus the ensemble values H_{ens} and ET$_{ens}$, For every statistical measure, TSEB-PT and TSEB-SW$_{Rc,VPD}$ have the best performance.

Another way to evaluate the different TSEB models in a more qualitative way is illustrated in Figs. 8, 9, and 10. In Figures 8 and 9, daytime H and LE from the different versions of TSEB versus the range of observed values derived from unclosed and the different closure methods is displayed along with the ensemble (average). A similar comparison is illustrated in Fig. 10 for daily ET. For each year, the model output from TSEB-PT or TSEB-SW$_{Rc,VPD}$

tend to fall within the range of uncertainty in the observed fluxes. In fact, more often both TSEB-PT or TSEB-SW$_{Rc,VPD}$ daytime H and LE and daily ET output come close to the ensemble values, while flux estimates from TSEB-PT$_{clim}$ and TSEB-PM$_{Rc,min}$ tend to fall outside the observed uncertainty range in the fluxes, except for year 2020, the year with the greatest advection.

The cases with significant advection causing $T_{RH} - T_{air} < 0$ under $R_N > 100$ W m^{-2} were selected to see how the different TSEB formulations could account for this excess heat enhancing LE/ET. In Fig. 11, it is quite clear that it is only the TSEB-PM$_{Rc,min}$ and TSEB-SW$_{Rc,VPD}$ versions of the model that can compute the dynamic range in excess sensible heat flux, while TSEB-PT and TSEB-PT$_{clim}$ are unable to compute the range in advected heat. This inability to capture the strongly advective cases does not appear to significantly affect the performance of TSEB-PT in general at this site. However it may be advantageous to adopt the TSEB-PM$_{Rc,min}$ or TSEB-SW$_{Rc,VPD}$ where more frequently significant advective conditions are known to exist.

Table 2 Statistical measures of model performance for the four different transpiration versions implemented in TSEB using the ensemble value for daytime H, H_{ens} (W m^{-2})

Model	Year	N	Bias	MAE	RMSE	r	d
TSEB-PT	2017	117	25	27	32	0.87	0.77
	2018	121	48	48	53	0.71	0.55
	2019	97	58	58	61	0.75	0.5
	2020	125	18	22	28	0.87	0.79
	All	457	36	37	45	0.83	0.69
TSEB-PT$_{clim}$	2017	117	47	47	51	0.87	0.62
	2018	121	65	65	71	0.55	0.47
	2019	97	83	83	86	0.74	0.39
	2020	125	48	48	52	0.88	0.58
	All	457	60	60	66	0.8	0.59
TSEB-PM$_{Rc,min}$	2017	117	66	66	68	0.89	0.55
	2018	121	84	84	90	0.5	0.41
	2019	97	112	112	117	0.58	0.32
	2020	125	55	55	57	0.91	0.61
	All	457	77	77	84	0.67	0.51
TSEB-SW$_{Rc,VPD}$	2017	117	43	43	44	0.96	0.72
	2018	121	63	63	66	0.86	0.53
	2019	97	63	63	66	0.77	0.49
	2020	125	31	32	36	0.92	0.75
	All	457	49	49	54	0.89	0.67

$$\text{bias} = \sum_{i=1}^{N} O_i - P_i, \text{MAE} = \sum_{i=1}^{N} |O_i - P_i| \text{RMSE} = \left[\frac{1}{N}\sum_{i=1}^{N}\left(O_i - P_i\right)^2\right]^{1/2},$$
$$r = \frac{\sum_{i=1}^{N}\left(P_i - \bar{P}\right)\left(o_i - \bar{o}\right)}{\left[\sum_{i=1}^{N}\left(o_i - \bar{o}\right)^2\sum_{i=1}^{N}\left(P_i - \bar{o}\right)^2\right]^{1/2}}, d = 1 - \frac{\sum_{i=1}^{N}\left(P_i - O_1\right)^2}{\sum_{i=1}^{N}\left(\left|P_i - \bar{o}\right| + \left|o_i - \bar{o}\right|\right)^2}.$$

The column headers are defined as N (number of observations), bias (model-observed differences), mean absolute error (MAE), root mean square error (RMSE), r is the correlation coefficient and d is the index of agreement. Equations for the different statistical measures are provided in the table footnote where the symbol O is the observed value and P is the model predicted value

Conclusions

The original and three other transpiration formulations for the TSEB model were evaluated for a vineyard site near Fresno CA having significant advection of heat occurring on multiple occasions depending on the management of the vine biomass and atmospheric demand. The original TSEB-PT version using the Priestley–Taylor evaporation equation for unstressed vine transpiration and the TSEB-SW$_{Rc,VPD}$ version that uses transpiration and soil evaporation algorithms of Shuttleworth and Wallace (1985), along with a minimum canopy resistance formulation that is a function of VPD, yielded the best agreement with observed average daytime H and LE as well as daily ET.

The other two transpiration formulations, using an adjusted Priestley–Taylor α_{PT} coefficient accounting for the more arid conditions and higher evaporative demand based on climatology and the TSEB-PM$_{Rc,min}$ based on Penman–Monteith big-leaf model of canopy transpiration having a minimum canopy resistance value for unstressed vegetation, did not perform as well. Both models tended to overestimate LE/ET and underestimate H and only under the more extreme advective conditions (in years 2017 and 2020) did these two approaches yield comparable results with original Priestley–Taylor and Shuttleworth–Wallace schemes.

A future analysis will evaluate these different transpiration formulations over other GRAPEX vineyard sites in different climates and for different vine varieties. We will particularly focus on how well the TSEB-based Shuttleworth–Wallace scheme performs without requiring local calibration of the canopy conductance model for different vine varieties (Fig. 5). Initial results comparing Chardonnay and Merlot varieties suggests the 1/T versus 1/VPD formulation may not vary significantly and that TSEB-based Shuttleworth–Wallace scheme may not be highly sensitive to the derived coefficients in Eq. (5). If found to be robust without local calibration, this formulation may have greater utility in the regional modeling than using the original TSEB-PT land surface scheme when applied in vineyards in strongly advective environments (Knipper et al. 2020).

Table 3 Statistical measures of model performance for the four different transpiration versions implemented in TSEB using the ensemble value for daily ET, ET_{ens} (mm day^{-1})

Model	Year	N	Bias	MAE	RMSE	r	d
TSEB-PT	2017	116	−0.3	0.4	0.5	0.92	0.94
	2018	120	−1	1	1	0.94	0.8
	2019	96	−0.6	0.6	0.7	0.9	0.84
	2020	124	−0.2	0.4	0.5	0.92	0.95
	All	453	−0.5	0.6	0.7	0.91	0.9
TSEB-PT$_{clim}$	2017	116	−0.9	0.9	1	0.9	0.8
	2018	120	−1.4	1.4	1.5	0.89	0.67
	2019	96	−1.4	1.4	1.4	0.9	0.63
	2020	124	−1.1	1.1	1.2	0.93	0.8
	All	453	−1.2	1.2	1.3	0.91	0.77
TSEB-PM$_{Rc,min}$	2017	116	−0.8	0.9	1	0.9	0.83
	2018	120	−1.4	1.4	1.5	0.9	0.68
	2019	96	−1.7	1.7	1.8	0.81	0.56
	2020	124	−0.6	0.7	0.8	0.92	0.9
	All	453	−1.1	1.1	1.3	0.85	0.76
TSEB-SW$_{Rc,VPD}$	2017	116	−0.3	0.4	0.5	0.93	0.95
	2018	120	−0.9	0.9	1	0.95	0.82
	2019	96	−0.4	0.4	0.5	0.92	0.91
	2020	124	0	0.3	0.4	0.94	0.97
	All	453	−0.4	0.5	0.7	0.9	0.92

The column definitions are defined as *N* (number of observations), *bias* (model-observed differences), mean absolute error (*MAE*), root mean square error (*RMSE*), *r* is the correlation coefficient and *d* is the index of agreement. See Table 2 for equations
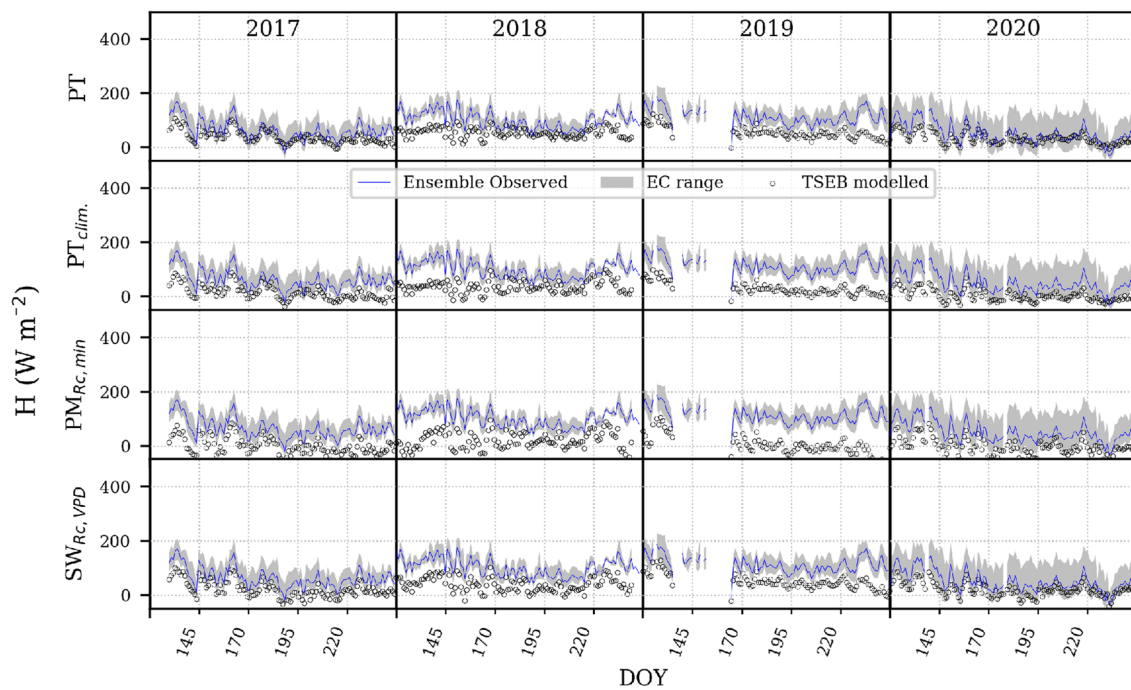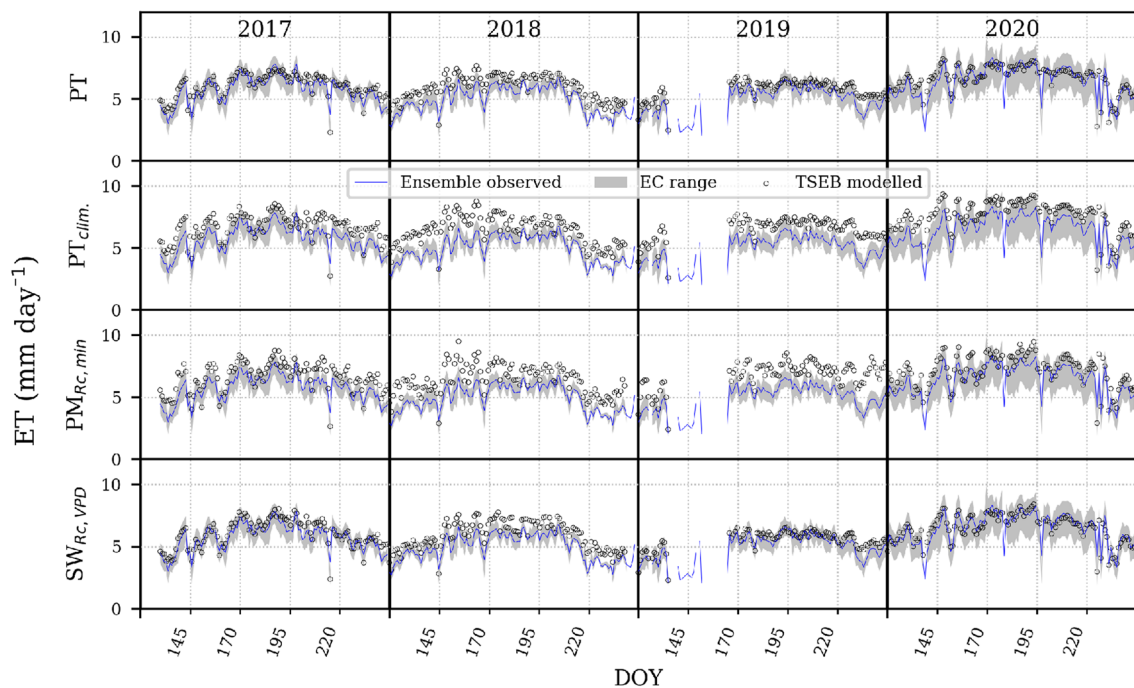

Fig. 8 Daytime average *H* plots computed using the four transpiration formulations in TSEB (open black circles) compared to the four different estimates of the actual daytime average *H*. The shaded area represents the range in observed *H* produced by the Bowen ratio and residual closure methods and the unclosed measurements while the blue line is the ensemble or average of the three estimates of actual *H* (colour figure online)
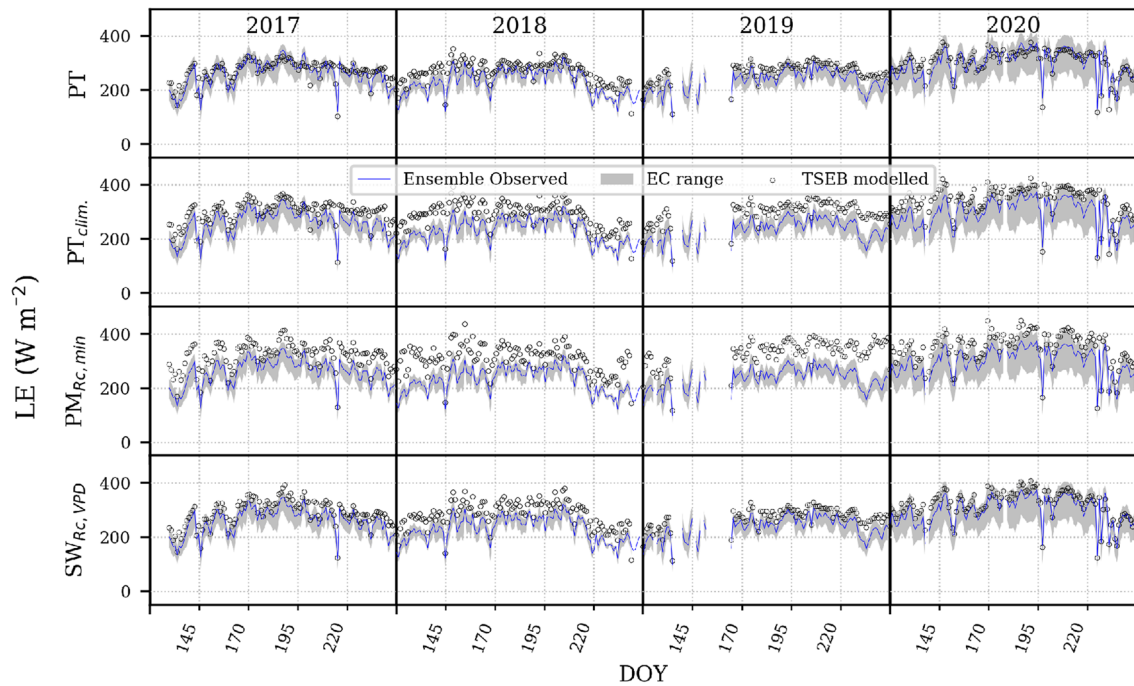
Fig. 9 Daytime average LE plots computed using the four transpiration formulations in TSEB (open black circles) compared to the four different estimates of the actual daytime average LE. The shaded area represents the range in observed LE produced by the Bowen ratio and residual closure methods and the unclosed measurements while the blue line is the ensemble or average of the three estimates of actual LE (colour figure online)

Fig. 10 Daily ET computed using the four transpiration formulations in TSEB (open black circles) compared to the four different estimates of the actual daily ET. The shaded area represents the range in observed daily ET produced by the Bowen ratio and residual closure methods and the unclosed measurements while the blue line is the ensemble or average of the three estimates of actual daily ET (colour figure online)
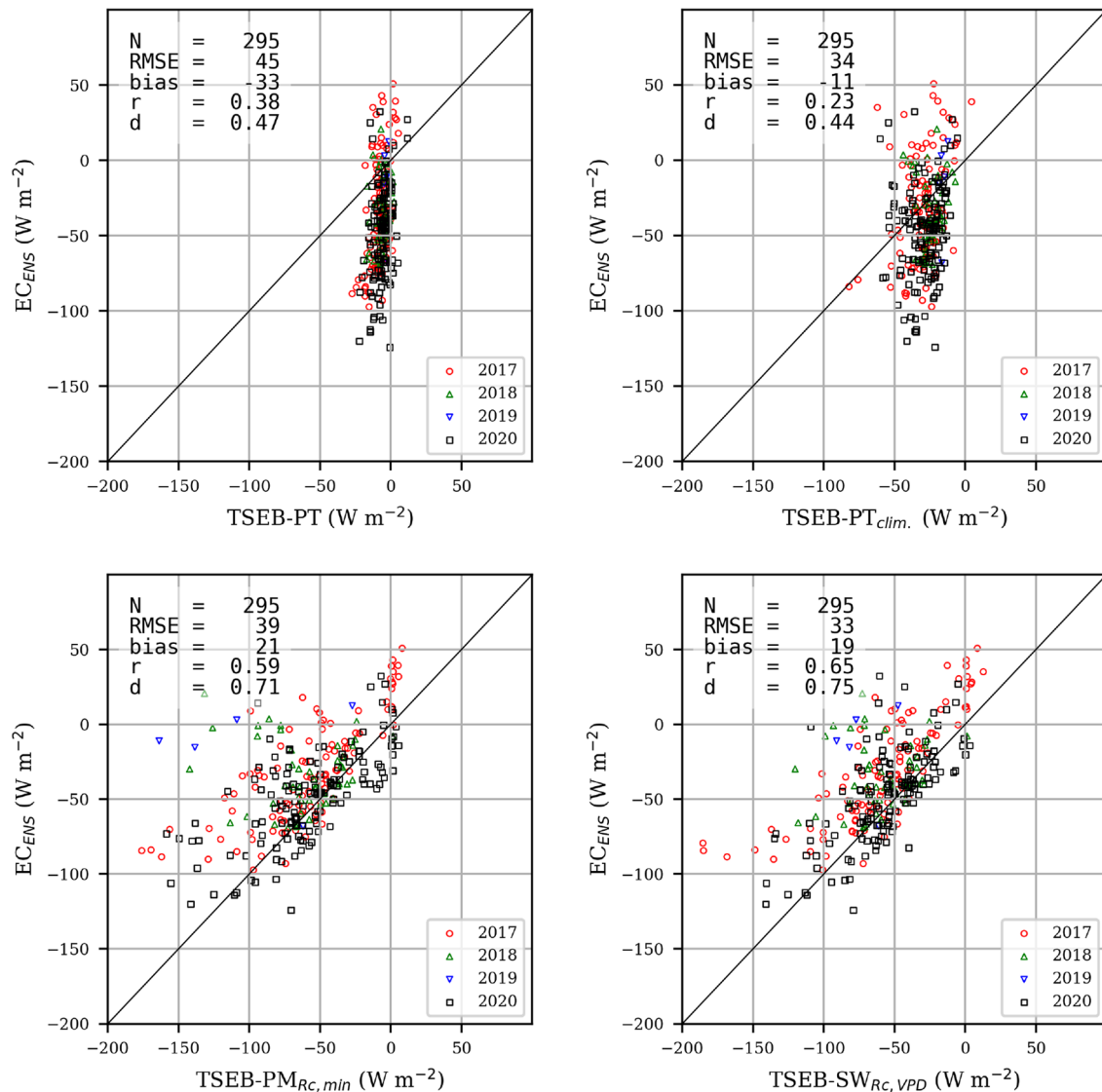
Fig. 11 Observed vs. Predicted validation scatterplots for the hourly sensible heat fluxes (H) with significant advection (i.e., $T_{rad} - T_{air} < 0$ and $Rn > 100$), for the four versions of the transpiration formulation in TSEB. Observed values are considered as the ensemble or average of the three estimates of actual hourly sensible heat flux. Blue dots represent cases for 2017, green upward triangles for 2018, blue down-

ward triangles for 2019, and black squares for 2020. Each plot also shows a table with the error and agreement statistics: N is the number of valid cases, $RMSE$ is the root mean square error, $bias$ is the mean difference between the observed and the predicted, r is the correlation coefficient between observed and predicted and d is the Willmott's Index of Agreement (colour figure online)

Declarations

Conflict of interest On behalf of all authors, the corresponding author states that there is no conflict of interest.

References

Agam N, Kustas WP, Anderson MC, Norman JM, Colaizzi PD, Howell TA, Prueger JH, Meyers TP, Wilson TB (2010) Application of the Priestley-Taylor approach in a two-source surface energy balance model. J Hydromet 11:185–198

Agam N, Kustas WP, Alfieri JG, Gao F, McKee LM, Prueger JH, Hipps LE (2019) Micro-scale spatial variability in soil heat flux (SHF) in a wine-grape vineyard. Irrig Sci 37:253–268. https://doi.org/10.1007/s00271-019-00634-6

Alfieri JG, Kustas WP, Prueger JH, McKee LG, Hipps LE, Gao F (2019) A multi-year intercomparison of micrometeorological observations at adjacent vineyards in California's central valley during GRAPEX. Irrig Sci 37:345–357. https://doi.org/10.1007/s00271-018-0599-3

Allen RG, Pruitt WO, Wright JL, Howell TA, Ventura F, Snyder R et al (2006) (2006) A recommendation on standardized surface resistance for hourly calculation of reference ETo by the FAO56 Penman-Monteith method. Agric Water Manag 81:1–22

Bambach N, Alfieri JG, Prueger JH, Kustas WP, Alsina MM, Hipps LE, McKee LM, Castro-Bustamante S, McElrone, AJ (2022) Canopy level evapotranspiration uncertainty: The impact of different data processing and energy budget closure methods Irrg Sci **(in review)**

Brutsaert W (1982) Evaporation into the atmosphere, theory, history and applications. D. Reidel, Boston, p 299

Brutsaert W, Stricker H (1979) An advection-aridity approach to estimate actual regional evapotranspiration. Water Resour Res 15:443–450. https://doi.org/10.1029/WR015i002p00443

Cammalleri C, Anderson MC, Kustas WP (2014) Upscaling of evapotranspiration fluxes from instantaneous to daytime scales for thermal remote sensing applications. Hydrol Earth Sys Sci 18:1885–1894. https://doi.org/10.5194/hess-18-1885-2014

Claverie M, Ju J, Masek JG, Dungan JL, Vermote EF, Roger J-C, Skakun SV, Justice C (2018) The Harmonized Landsat and Sentinel-2 surface reflectance data set. Remote Sens Environ 219:145–161. https://doi.org/10.1016/j.rse.2018.09.002

Colaizzi PD, Evett SR, Howell TA, Tolk JA (2006) Comparison of five models to scale daily evapotranspiration from one-time-of-day measurements. Tran ASABE 49(5):1409–1417

Colaizzi PD, Kustas WP, Anderson MC, Agam N, Tolk JA, Evett SR, Howell TA, Gowda PH, O'Shaughnessy SA (2012) Two-source energy balance model estimates of evapotranspiration using component and composite surface temperatures. Adv Water Resour 50:134–151

Colaizzi PD, Agam N, Tolk JA, Evett SR, Howell TA, Gowda PH, O'Shaughnessy SA, Kustas WP, Anderson MC (2014) Two source energy balance model to calculate E, T, and ET: comparison of Priestley-Taylor and Penman-Monteith formulations and two time scaling methods. Trans ASABE 57(2):479–498

Fisher JB, Tu KP, Baldocchi DD (2008) Global estimates of the land–atmosphere water flux based on monthly AVHRR and ISLSCP-II data, validated at 16 FLUXNET sites. Remote Sens 112(3):901–919

Gao F, Anderson MC, Daughtry CS, Karnieli A, Hively WD, Kustas WP (2020) A within-season approach for detecting early growth stages in corn and soybean using high temporal and spatial resolution imagery. Remote Sens Environ 242:11752. https://doi.org/10.1016/j.rse.2020.111752

Grossiord C, Buckley TN, Cernusak LA, Novick KA, Poulter B, Siegwolf RT, Sperry JS, McDowell NG (2020) Plant responses to rising vapor pressure deficit. New Phytol 226(6):1550–1566. https://doi.org/10.1111/nph.16485

Huete A, Didan K, Miura T, Rodriguez EP, Gao X, Ferreira LG (2002) Overview of the radiometric and biophysical performance of the MODIS vegetation indices. Remote Sens Environ 83:195–213. https://doi.org/10.1016/S0034-4257(02)00096-2

Huntington JL, Szilagyi J, Tyler SW, Pohll GM (2011) Evaluating the complementary relationship for estimating evapotranspiration from arid shrublands. Water Resour Res 47:W05533. https://doi.org/10.1029/2010WR009874

Jarvis PG (1976) The interpretation of the variations in leaf water potential and stomatal conductance found in canopies in the field. Phil Trans R Soc Lond B 273:593–610. https://doi.org/10.1098/rstb.1976.0035

Jarvis PG, McNaughton KG (1986) Stomatal control of transpiration - scaling up from leaf to region. Adv Ecol Res 15:1–49

Kahler DM, Brutsaert W (2006) Complementary relationship between daily evaporation in the environment and pan evaporation. Water Resour Res 42:W05413. https://doi.org/10.1029/2005WR004541

Kang Y, Gao F, Anderson MC, Kustas WP, Nieto H, Knipper K, Yang Y, White A, Torres-Rua A, Alsina M, Karneli A (2022) Evaluation of satellite leaf area index in California vineyards for improving water use estimation. Irrig Sci **(in review)**

Knipper K, Kustas WP, Anderson MC, Alsina M, Hain C, Alfieri JG, Prueger JH, Gao F, McKee LG, Sanchez L (2019) Using high-spatiotemporal thermal satellite ET retrievals for near-real time water use and stress monitoring in a California vineyard. Remote Sens 11:2124. https://doi.org/10.3390/rs11182124

Knipper KR, Kustas WP, Anderson MC, Alfieri JG, Prueger JH, Hain CR, Gao F, McKee LM, Alsina MM, Sanchez L (2020) Using high-spatiotemporal thermal satellite ET retrievals to monitor water use over California vineyards of different climate, vine variety and trellis design. Agric Water Manag. https://doi.org/10.1016/j.agwat.2020.106361

Kustas WP, Anderson MC (2009) Advances in thermal infrared remote sensing for land surface modeling. Agric For Meteorol 149:2071–2081

Kustas WP, Norman JM (1999) Evaluation of soil and vegetation heat flux predictions using a simple two-source model with radiometric temperatures for partial canopy cover. Agric For Meteorol 94:13–29

Kustas WP, Anderson MC, Alfieri JG, Knipper K, Torres-Rua A, Parry CK, Nieto H, Agam N, White A, Gao F, McKee L, Prueger JH, Hipps LE, Los S, Alsina M, Sanchez L, Sams B, Dokoozlian N, McKee M, Jones S, McElrone A, Heitman JL, Howard AM, Post K, Melton F, Hain C (2018) The grape remote sensing atmospheric profile and evapotranspiration eXperiment (GRAPEX). Bull Am Meteorol Soc 9:1791–1812. https://doi.org/10.1175/BAMS-D-16-0244.1

Kustas WP, Agam N, Ortega-Farias S (2019a) Forward to the GRAPEX special issue. Irrig Sci. https://doi.org/10.1007/s00271-019-00633-7

Kustas WP, Alfieri JG, Nieto H, Gao F, Anderson MC, Prueger JH, Wilson TG (2019b) Utility of the two-source energy balance model TSEB in vine and inter-row flux partitioning over the growing season. Irrig Sci 37:375–388. https://doi.org/10.1007/s00271-018-0586-8

Leuning R (1995) A critical appraisal of a combined stomatal-photosynthesis model for C3 plants. Plant Cell Environ 18:339–355. https://doi.org/10.1111/j.1365-3040.1995.tb00370.x

Liu SM, Xu ZW, Wang WZ et al (2011) A comparison of eddy-covariance and large aperture scintillometer measurements with respect to the energy balance closure problem Hydrol Earth. Syst Sci 15:1291

Lohammar T, Larsson S, Linder S, Falk SO (1980) FAST: simulation models of gaseous exchange in scots pine. Ecol Bull 32:505–523

Mauder M, Foken T, Cuxart J (2020) Surface-energy-balance closure over land: a review. Bound Layer Meteorol. https://doi.org/10.1007/s10546-020-00529-6

Melton F, Huntington JL, Grimm R, Herring J, Hall M, Rollison D, Erickson T, Allen R, Anderson M, Blankenau P et al (2022) OpenET—filling the biggest data gap in water management for the Western U.S. J Am Water Resour Assoc, 1–24. https://doi.org/10.1111/1752-1688.12956

Monteith JL (1995) A reinterpretation of stomatal responses to humidity. Plant Cell Environ 18:357–364. https://doi.org/10.1111/j.1365-3040.1995.tb00371.x

Nassar A, Torres-Rua A, Kustas W, Alfieri J, Hipps L, Prueger J, Nieto H, Alsina MM, White W, McKee L (2021) Assessing daily evapotranspiration methodologies from one-time-of-day sUAS and EC Information in the GRAPEX project. Remote Sens 13:2887. https://doi.org/10.3390/rs13152887

Nieto H, Kustas WP, Torres-Rúa A, Alfieri JG, Gao F, Anderson MC, White WA, Song L, del Mar AM, Prueger JH, McKee M, Elarab M, McKee LG (2019a) Evaluation of TSEB turbulent fluxes using different methods for the retrieval of soil and canopy component temperatures from UAV thermal and multispectral imagery. Irrig Sci 37:389–406. https://doi.org/10.1007/s00271-018-0585-9

Nieto H, Kustas WP, Alfieri JG, Gao F, Hipps LE, Los S, Prueger JH, McKee LG, Anderson MC (2019b) Impact of different within canopy wind attenuation formulations on modelling sensible heat flux using TSEB. Irrig Sci 37:315–331. https://doi.org/10.1007/s00271-018-0611-y

Nieto H, Alsina MM, Kustas WP, Garcia-Tejera O, Chen F, Bambach N, Gao F, Alfieri JG, Hipps LE, Prueger JH, McKee LG, Zahn E, Bou-Zeid E, McElrone A, Castro S, Dokoozlian N (2022) Evaluating different metrics from the thermal-based two-source energy balance model for monitoring grapevine water stress Irrig Sci (in review)

Norman JM, Kustas WP, Humes KS (1995) Source approach for estimating soil and vegetation energy fluxes in observations of directional radiometric surface temperature. Agric For Meteorol 77(3–4):263–293

Parry CK, Nieto H, Guillevic P, Agam N, Kustas WP, Alfieri JG, McKee L, McElrone AJ (2019) An intercomparison of radiation partitioning models in vineyard canopies. Irrig Sci. https://doi.org/10.1007/s00271-019-00621-x

Priestley CHB, Taylor RJ (1972) On the assessment of surface heat flux and evaporation using large-scale parameters. Mon Weather Rev 100(2):81–92

Shuttleworth WJ, Wallace JS (1985) Evaporation from sparse crops-an energy combination theory. Q J R Meteorol Soc 111:839–855. https://doi.org/10.1002/qj.49711146910

Szilagyi J (2007) On the inherent asymmetric nature of the complementary relationship of evaporation. Geophys Res Lett 34:L02405. https://doi.org/10.1029/2006GL028708

Thomas C, Martin J, Goeckede M, Siqueira M, Foken T, Law B, Loescher H, Katul G (2008) Estimating daytime subcanopy respiration from conditional sampling methods applied to multiscalar high frequency turbulence time series. Agric for Meteorol 148(8):1210–1229

Twine TE, Kustas WP, Norman JM, Cook DR, Houser PR, Meyers TP, Prueger JH, Starks PJ, Wesely ML (2000) Correcting eddy-covariance flux underestimates over a grassland. Agric For Meteorol 103:279–300

White WA, Alsina MM, Nieto H, McKee LG, Gao F, Kustas WP (2018) Determining a robust indirect measurement of leaf area index in California vineyards for validating remote sensing-based retrievals. Irrig Sci. https://doi.org/10.1007/s00271-018-0614-8

Xu Z, Ma Y, Liu S et al (2017) Assessment of the energy balance closure under advective conditions and its impact using remote sensing data. J Appl Meteorol Climatol 56:127–140. https://doi.org/10.1175/JAMC-D-16-0096.1

Zahn E, Bou-Zeid E, Good S, Katul GG, Thomas C, Ghannam K, Smith JA, Chamecki M, Dias NL, Fuentes JD, Alfieri JG, Kwon H, Caylor K, Gaom Z, Soderberg K, Bambach NE, Hipps LE, Prueger JH, Kustas WP (2022) Direct partitioning of eddy-covariance water and carbon dioxide fluxes into ground and plant components. Agric Forest Meteorol 315:108790. https://doi.org/10.1016/j.agrformet.2021.108790

Authors and Affiliations

William P. Kustas[1] · **Hector Nieto**[2,3] · **Omar Garcia-Tejera**[4] · **Nicolas Bambach**[5] · **Andrew J. McElrone**[6,7] · **Feng Gao**[1] · **Joseph G. Alfieri**[1] · **Lawrence E. Hipps**[8] · **John H. Prueger**[9] · **Alfonso Torres-Rua**[10] · **Martha C. Anderson**[1] · **Kyle Knipper**[11] · **Maria Mar Alsina**[12] · **Lynn G. McKee**[1] · **Einara Zahn**[13] · **Elie Bou-Zeid**[13] · **Nick Dokoozlian**[12]

[1] USDA-ARS, Hydrology and Remote Sensing Laboratory, Beltsville, MD, USA

[2] Complutum Tecnologías de la Información Geográfica S.L. Madrid, Madrid, Spain

[3] Plant Protection Department, Institute of Agricultural Sciences-CSIC, Madrid, Spain

[4] Department of Agronomy, Institute for Sustainable Agriculture-CSIC, Córdoba, Spain

[5] Department of Land, Air and Water Resources, University of California, Davis, CA, USA

[6] USDA-ARS Crops Pathology and Genetics Research Unit, Davis, CA, USA

[7] Department of Viticulture and Enology, University of California, Davis, CA, USA

[8] Department of Plants Soils and Climate, Utah State University, Logan, UT, USA

[9] USDA-ARS, National Laboratory for Agriculture and the Environment, Ames, IA, USA

[10] Department of Civil and Environmental Engineering, Utah State University, Logan, UT, USA

[11] USDA-ARS, Sustainable Agricultural Water Systems Unit, Davis, CA, USA

[12] E & J Gallo Winery, Viticulture, Chemistry and Enology, Modesto, CA, USA

[13] Department of Civil and Environmental Engineering, Princeton University, Princeton, NJ, USA